



# Correlations of Undrained Shear Strength Based on CPTu Tests for Clayey Soils in Macau

Junwu Zhang<sup>1</sup>, Yuliang Chen<sup>1</sup>, Guanzheng Wu<sup>2,3,4</sup>, Lei Li<sup>2,3,4\*</sup>, Ziming Zeng<sup>2,3,4</sup>

<sup>1</sup>China Road & Bridge Corporation, No.88 C, Andingmenwai Avenue, Beijing 100011, China

<sup>2</sup>Guangzhou Construction Co. Ltd., No. 4 Guangwei Road, Yuexiu District, Guangzhou 510030, China

<sup>3</sup>Guangzhou Municipal Construction Group Co. Ltd., No. 4 Guangwei Road, Yuexiu District, Guangzhou 510030, China

<sup>4</sup>Guangzhou Design Institute Group Co. Ltd., 3 Tiyu-Dongheng Street, Guangzhou 510620, China

\*Correspondence: lilei@gzdi.com

**Abstract.** For decades, studies have used a semi-empirical method to correlate the undrained shear strength ( $s_u$ ) of clay with CPTu profiles; however, extensive experimental data indicate significant variability in the cone factors used in these correlations, which leads to uncertainty in interpreting  $s_u$  from CPTu results. To address this issue further, this paper collected two types of in-situ experimental data from a coastal area in Macau, including 10 CPTu tests and 13 VST tests. By synthesizing existing research on correlations between CPTu results and  $s_u$ , a method is introduced that incorporates soil classification before conducting correlation analysis, resulting in the derivation of more accurate cone factors. Various correlation methods and CPTu reading profile ranges are compared. It is derived that, when interpreting  $s_u$  from CPTu data: the application of ( $q_t - u_2$ ) is not recommended; the range of CPTu profile corresponding to the length of the shear vane is more suitable than other longer ranges.

**Keywords:** piezocone penetration test (CPTu); undrained shear strength; Macau; soil behavior type index; correlation analysis

## 1 Introduction

Measuring the shear strength of clay is crucial in geotechnical engineering because it determines key parameters such as the internal friction angle and the shear modulus, significantly impacting engineering design and construction. Methods for determining shear strength include the direct shear test, the triaxial compression test, the vane shear test, and the cone penetration test with pore pressure measurement (also known as the piezocone penetration test, CPTu). CPTu primarily assesses shear strength in an undrained condition, as it is performed quickly, preventing the drainage of pore water in fine-grained soils [1,2].

However, the data directly obtained from CPTu generally include cone resistance ( $q_c$ ), friction sleeve resistance ( $f_s$ ), and pore water pressure ( $u_2$ ). To interpret other soil parameters, like the undrained shear strength ( $s_u$ ), from these measurements, additional research into correlations is necessary. Lunne et al. have mentioned that both theoretical solutions and empirical methods exist for evaluation of soil parameters from cone penetration data [3]. Theoretical methods, including cavity expansion theory [4-6], strain path theory [7], and numerical approaches [8-10], which consider parameters such as undrained modulus ( $E_u$ ) and stiffness index ( $I_r$ ), manifest as more complex expressions. In contrast, other theoretical approaches based on bearing capacity [11,12] are more applied due to their simplicity and similarity to the empirical methods:

$$q_c = N_c s_u + \sigma_{vo}, \quad (1)$$

where  $q_c$  is the bearing capacity of the cone,  $N_c$  is a theoretical cone factor and  $\sigma_{vo}$  is the in situ total stress.

Numerous studies have aimed at estimating cone factors to define undrained shear strength [13-15]. These cone factors can be categorized into groups based on the data used: the total cone resistance, the net cone resistance, and the effective cone resistance, etc. Researchers have not reached a consensus on the values of these factors due to significant scatter. Several influencing factors, including sampling and testing methods, boundary conditions, loading direction, loading rate, stress level, and disturbance effects, were identified by Kulhawy and Mayne during their investigation of the calibration procedures for cone factors in the lab [16]. Furthermore, the laboratory test methods used to determine results compared with CPTu data have come in various forms, including unconfined compression, triaxial, and vane tests, etc [16,17]. This diversity further complicates the accurate definition of the cone factor range.

Considering CPTu as an in-situ testing method, directly comparing its data with in-situ undrained shear strength measurements can circumvent the aforementioned interference factors and shall yield more accurate correlation results. To accomplish this goal, data from 10 CPTu tests and 13 field vane shear tests (VST) are selected from a specific coastal region in Macau. Our focus is on determining the undrained shear strength of the clayey soils. By reviewing existing methods on the correlations between CPTu results and undrained shear strength, we compare the outcomes of CPTu and in-situ VST tests. To align two different test results conducted at different locations, a new pairing method is developed. After pairing the data, a "classification first, correlation later" approach is introduced, leading to improved correlation results. Recommendations are made for the classification criteria of the soils in this study. Finally, we compared the performance of different correlation methods, and the results indicate that using the net cone resistance to estimate  $s_u$  yields the best outcomes. Additionally, the influence of the CPTu reading profile range on the correlation is dependent on the soil type.

## 2 Field Test Program

### 2.1 Site Background

The geological survey for this project covers the coastal area adjacent to the western channel of Cotai, Macau, originally a marine area (see Figure 1). Due to Macau's limited land availability, the government reclaimed this section, forming what is now Cotai. Survey data revealed that the geological stratification of the site—shaped by both natural and human activities—primarily consists of, in sequence: back-filled soil, marine depositional clay, alluvial clay, alluvial sand, residual soil, and layers of completely and moderately weathered granite. This study focuses on the marine depositional clay and the alluvial clay, where both VST and CPTu data were collected.



Fig. 1. Approximate scope of the study

The marine depositional layer is characterized by extremely soft to soft clayey soil. This soil is saturated, stable, and locally weak. The cross-sections exhibit relatively uniform soil composition, while occasional shell fragments and humic materials are observed. The layer thickness ranges from approximately 8.50 to 12.50 meters, with top elevations from +0.99 to -6.38 meters above sea level. The average standard penetration test value is 3.24.

The alluvial clay layer is saturated, dense to very dense, and locally stable. Its surface is relatively smooth, with fairly uniform soil composition, containing minor amounts of sand and calcareous nodules. The average standard penetration test value is 13.90.

The statistical values of some other geological characteristics of the clayey soils are presented in Table 1, while the grain size distributions of the clayey soils are shown in Table 2.

**Table 1.** Statistical Values of Characteristic Parameters of Clay.

Soil Type	Statistical Values	$\gamma_n$ (kN/m <sup>3</sup> )	$w_n$ (%)	$w_L$ (%)	$w_P$ (%)	$I_P$
Marine Depositional Clay	Number of tests	13	13	14	14	14
	Max	19.4	61.4	84.0	47.0	41.0
	Min	16.2	53.1	55.0	30.0	23.0
	Mean	17.1	53.0	70.7	39.9	31.2
Alluvial Clay	Number of tests	19	17	19	19	19
	Max	20.2	53.9	80.0	49.0	42.0
	Min	16.9	27.2	44.0	16.0	17.0
	Mean	18.2	40.2	58.3	31.0	25.6

**Table 2.** Grain Size Distribution of Clay (%)

Soil Type	Gravel	Sand	Silt	Clay
Marine Depositional Clay	0.04	14.9	18.2	66.9
Alluvial Clay	2.0	18.5	18.0	61.5

## 2.2 VST Tests

The plan view of the VST test locations is shown in Figure 3. The tests used a Geonor H10 vane borer produced by Geonor, Inc., with vane dimensions of either 65 x 130 mm or 50 x 100 mm.

All the tests were conducted in accordance with BS 1377: Part 9 [18], with the following test procedure: first, a pilot hole was drilled at the designated location to penetrate the upper fill soil, and the casing was inserted to the bottom of the borehole. Then, the vane was extended to the bottom through an extension rod and advanced at least 500 mm further into the soil, reaching the predetermined measurement depth. After connecting the vane apparatus and zeroing the gauge, the crank handle was rotated clockwise at a relatively constant rate of 0.1~0.2°/s. When the gauge reading reached its peak, the crank was rotated for an additional 1~2 minutes, and the peak reading was recorded as the shear strength of the intact soil. After completing the shear test at the current depth, the vane was further pushed into the soil to the next test depth, and the above steps were repeated until either the instrument's limit was exceeded or the soft clay layer was penetrated.

Detailed information and results of the VST tests can be found in Table S1 in the Supplementary Materials.

## 2.3 CPTu Tests

The plan view of the test locations is shown in Figure 3, involving 10 CPTu tests. The works were carried out in accordance with the ASTM Standard [19]. A 200kN RST-1

Penetrometer with GeoMil triple channel electrical piezocones was used during the test. The piezocone, with a tip area of 10cm<sup>2</sup> and a 150cm<sup>2</sup> friction sleeve, could measure the tip resistance ( $q_c$ ), the friction on the sleeve ( $f_s$ ), the relative cone inclination ( $I$ ) and the induced pore water pressure ( $u_2$ ), independently. The piezocones were initially calibrated in the GeoMil workshops in Holland, at which time they were temperature stabilised and corrected for the maximum length of sounding cable to be used.

Following positioning at the specified location, the CPTu test proceeded as follows: the piezocone was pushed into the ground at a constant rate of 20 mm/s by hydraulic rams mounted on the penetrometer frame; each penetration increment was 1.00 m, after completing each stroke, another sounding rod was added until the desired depth was achieved. During the penetration process, the data measured by the piezocone was transmitted to a computer via the cable and recorded

The results of the CPTu tests are generally shown in graphical format, indicating various measured parameters plotted against depth and/or reduced level (shown in Figure 2). Details of the tests can be found in Table S2 of the Supplementary Materials.

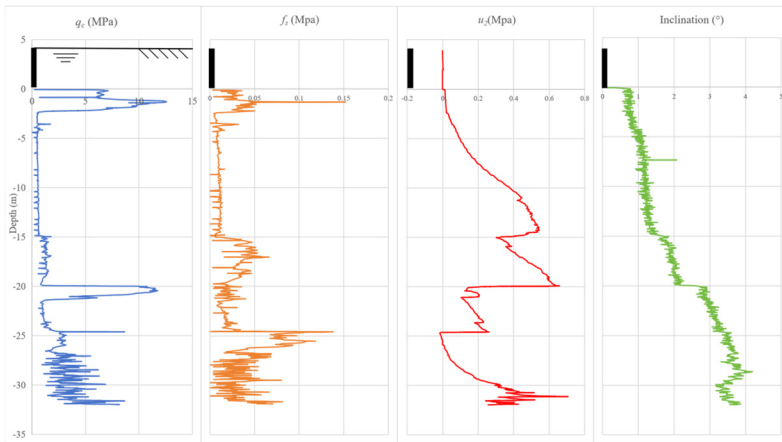


Fig. 2. A typical CPTu test profile

### 3 VST-CPTu Correlations

#### 3.1 Correlation Methods

The “total” cone resistance from CPTu data is used to calculate the undrained shear stress ( $s_u$ ) in the following form:

$$s_u = \frac{q_c - \sigma_{vo}}{N_k}, \tag{2}$$

where  $N_k$  is an empirical cone factor.

The corrected total cone resistance  $q_t$  is defined by:

$$q_t = q_c + (1 - a)u_2, \tag{3}$$

here,  $a$  = area ratio of the cone (cones with an area ratio of 0.85 has been used in this study). Thus, the correlation can be redefined as:

$$s_u = \frac{q_t - \sigma_{vo}}{N_{kt}}, \quad (4)$$

where  $N_{kt}$  is the corrected cone factor.

Campanella et al. proposed that the effective cone resistance ( $q_e$ ) should be used to calculate the undrained shear strength ( $s_u$ ) [20]. The expression is presented in the following form:

$$s_u = \frac{q_e}{N_{ke}} = \frac{q_t - u_2}{N_{ke}}, \quad (5)$$

where  $N_{ke}$  is the effective cone factor.

Although a simple linear relationship exists between the undrained shear strength ( $s_u$ ) and the readings obtained from CPTu tests according to Equations (2), (4), and (5), numerous experimental results, including Figure 5 in this study, indicate that this relationship exhibits significant scatter, regardless of the estimation method used. This scatter of the correlations might be due to the fact that ( $s_u$ ) alone does not fully represent soil strength. Factors such as soil type, penetration rate, and the reference test method likely influence the results [21]. Sowers suggested that soil classification could have a direct impact on cone factors [22]. Therefore, emphasis was placed on accurately determining the soil class.

Many studies on soil classification have primarily focused on defining the ‘‘Soil Behavior Type Index’’ ( $I_c$ ), using the normalized cone resistance ( $Q_t$ ), normalized friction ratio ( $F_r$ ) and a pore pressure coefficient ( $B_q$ ) [23,24]. These values could be defined as:

$$Q_t = \frac{q_t - \sigma_{vo}}{\sigma'_{vo}}, \quad (6)$$

$$F_r = 100 \frac{f_s}{q_t - \sigma_{vo}}, \quad (7)$$

$$B_q = \frac{u_2 - u_0}{q_t - \sigma_{vo}} = \frac{\Delta u}{q_t - \sigma_{vo}}, \quad (8)$$

where  $\sigma'_{vo}$  is the effective overburden stresses, and  $u_0$  is the static pore-water pressure.

Among those studies, the most widely used form of  $I_c$  was proposed by Robertson and Wride, which simplifies the contribution of the pore pressure ratio ( $B_q$ ) [25]. It can be expressed as follows:

$$I_c = \sqrt{(3.47 - \log Q_t)^2 + (1.22 + F_r)^2}. \quad (9)$$

(9)

Further research introduced the parameter  $Q_{tn}$  as an enhanced version of the normalized cone resistance, designed to replace  $Q_t$  by incorporating a variable stress exponent ( $n$ ) that varies depending on soil type or  $I_c$  [25-27], as illustrated in Equation (10):

$$Q_{tn} = \left( \frac{q_t - \sigma_{vo}}{P_{a2}} \right) \left( \frac{P_a}{\sigma'_{vo}} \right), \tag{10}$$

where

$$n = 0.381I_c + 0.05 \left( \frac{\sigma'_{vo}}{P_a} \right) - 0.15 \leq 1. \tag{11}$$

(11)

$P_a$  and  $P_{a2}$  are the reference pressures, with units that must match those of the quantities within the same parentheses, respectively (e.g. if  $\sigma'_{vo}$  is in kPa,  $P_a = 100$  kPa; if  $q_t$  and  $\sigma_{vo}$  are in MPa,  $P_{a2} = 0.1$  MPa).

The soil classification based on  $I_c$  can be plotted on a logarithmic coordinate system of  $Q_{tn}$  vs.  $F_r$ , defining Zones 2 to 7. And with the additional algorithm proposed by Mayne, defining the soils in Zone 1, 8, and 9, a complete Chart  $Q_{tn}$  vs.  $F_r$ , is formed (seen in Figure 6) [28].

### 3.2 Selection of VST-CPTu Pairs

In this study, the CPTu and VST test sites were spaced horizontally from one meter to several hundred meters. Additionally, CPTu data exhibits continuous profiles across the surveyed strata, whereas VST data comprises discrete measurements taken at specified depths. When conducting correlation analysis between CPTu and VST results, it is imperative to address variations both in spatial locations and data continuity.

The first step in pairing involves aligning the spatial locations horizontally. In accordance with Tobler's First Law of Geography ("everything is related to everything else, but near things are more related than distant things" [29]), data from the nearest multiple CPTu points to a specified VST point are selected. Subsequently, distance effects between these points are incorporated into the matching process. The detailed procedure is outlined as follows:

In the overall plan view, plot the locations of the CPTu and VST points. Connect every three nearest CPTu points with straight lines to form a non-overlapping grid (shown as Figure 3);

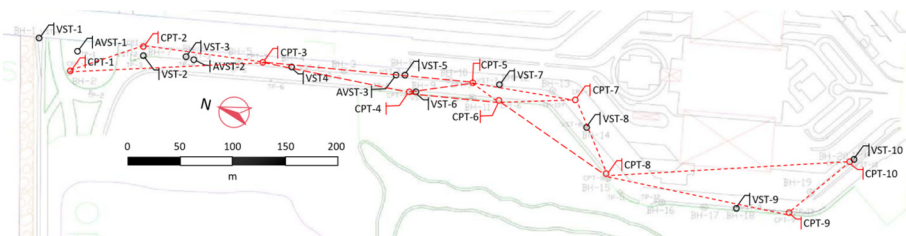


**Fig. 3.** Plan view of the test points

1. Examine each grid to identify the VST points within its boundaries. These VST points can be considered as being influenced and controlled by the three CPTu points (labeled as control points 1, 2, and 3) that form the vertices of the triangular grid;

2. Compute the horizontal distances ( $D_i, i=1, 2, 3$ ) from each VST point to control points 1, 2, and 3 within the grid. Assign a weight coefficient ( $W_{D_i}$ ) based on these distances, where

$$W_{D_i} \propto \frac{1}{D_i} \text{ and } \sum W_{D_i} = 1 \quad (12)$$

Thus, the CPTu data, such as  $q_c$ , can be calculated as a mapped value  $q_{c,VST}$  at the VST points:

$$q_{c,VST} = \sum W_{D_i} q_{ci} \quad (13)$$

Because VST-1, AVST-1, and VST-10 do not fall within any CPTu triangular grid, VST-1 and AVST-1 can be determined by CPT-1 and CPT-2, while VST-10 can be determined solely by CPT-10. The distances and weight coefficients for the test points within the grid can be found in Table S3 of the Supplementary Materials.

The second step of data pairing involves vertical matching. Following the recommendations of Macedo et al. [30], a “filtering window” is employed to delineate the range of selected CPTu profiles (shown in Figure 4, filtering  $q_c$  as an example). In this study, the filtering windows adopt three vertical ranges: one time, two times, and three times the length of the shear vane  $L$ . When  $L$  is used as the range, the vertical position of selected CPTu profiles correspond to the elevation of the shear vane in a VST test; when  $2L$  is used, the selected CPTu profile range extends  $0.5L$  above and below the shear vane’s range; and when  $3L$  is used, the selected CPTu profile range extends  $L$  above and below the shear vane’s range.

Additionally, excluding outliers is beneficial in safeguarding correlations from the influence of atypical values. For each segment of selected CPTu profiles, calculate their mean and standard deviation. Remove any data points from the dataset that differ from the mean by more than two standard deviations, classifying them as outliers. Finally, compute the mean of the filtered data, which could represent the value of CPTu data corresponding to the VST test.

In Figure 4, it is evident that the left CPTu profile shows stability, with the representative CPTu values derived from different filtering window lengths aligned closely and displaying sensitivity to outliers. In contrast, the right CPTu profile exhibits significant variation, resulting in noticeably different representative CPTu values across different filtering window lengths and reduced sensitivity to outliers. Therefore, Macedo et al. recommend prioritizing layers with stable CPTu values and recommend using layers where data does not exceed 30% of the average value within the studied depth ranges [30]. However, in practical applications, ensuring that each VST test occurs solely in uniformly stable strata is challenging. The 93 datasets obtained in this study did not exclude cases where CPTu profiles exhibited significant variation.

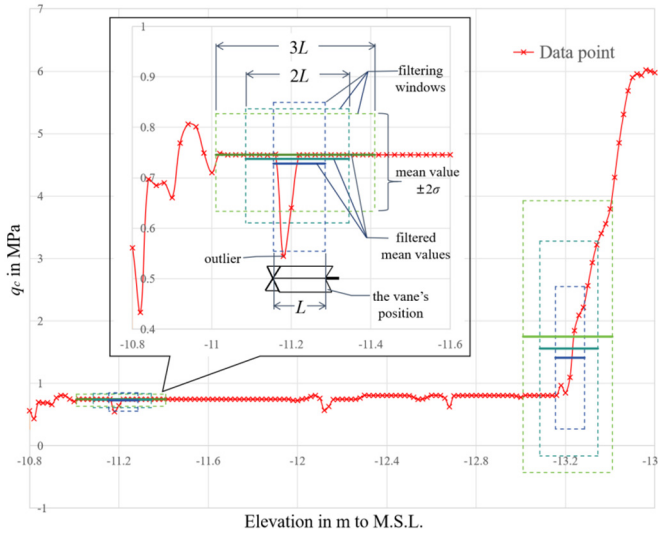


Fig. 4. Screening of  $q_c$  shown in a CPTu profile

### 3.3 Resluts of Correlations

After completing the VST-CPTu data pairing, the data points are plotted in a coordinate system, with CPTu readings on the x-axis and  $s_u$  on the y-axis. The inverse of the slope of a straight line drawn from each point to the origin (0,0) represents the actual cone factor for that point. Taking Figure 5 as an example, the x-axis represents  $(q_t - \sigma_{vo})$  filtered through a filtering window of length  $L$ , while the y-axis represents  $s_u$ . According to Equation (4), the cone factor  $N_{kt}$  ranges from 5.60 to 59.40, indicating significant variability, which is consistent with previous research. Furthermore, the linear regression of these points yields an  $R^2$  value of  $-0.654 < 0$ , suggesting that the linear relationship defined by Equation (4) cannot yield relatively accurate predictions of  $s_u$ .

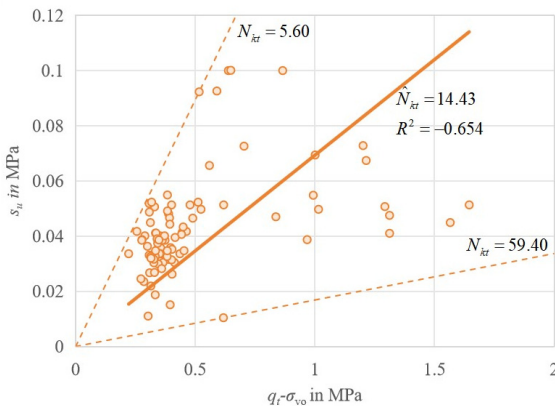


Fig. 5.  $s_u$  vs.  $(q_t - \sigma_{vo})$  by the filtering window length  $L$

To obtain more practical ranges of cone factors, it is necessary to first classify all points. The VST-CPTu correlation points are plotted on the Roberston  $Q_{tn}$  vs.  $F_r$  chart, as shown in Figure 6. It can be observed that within the scope of investigation, the soil types appear relatively homogeneous, with only a few classified as Silt Mixes (Zone 4:  $2.60 < I_c \leq 2.95$ ) or Organic Soils (Zone 2:  $I_c > 3.60$ ), while the majority are Clays (Zone 3:  $2.95 < I_c \leq 3.60$ ). However, this study does not strictly follow the  $I_c$  boundary values specified by Robertson [26]; instead, it relies more on the distribution characteristics of the points. The 17 points marked with blue triangles above, which have  $I_c$  values less than 3.25~3.26, are relatively dispersed and grouped as one set, while the remaining points marked with orange circles below, which have  $I_c$  values greater than 3.25~3.26, are more concentrated and grouped as another set.

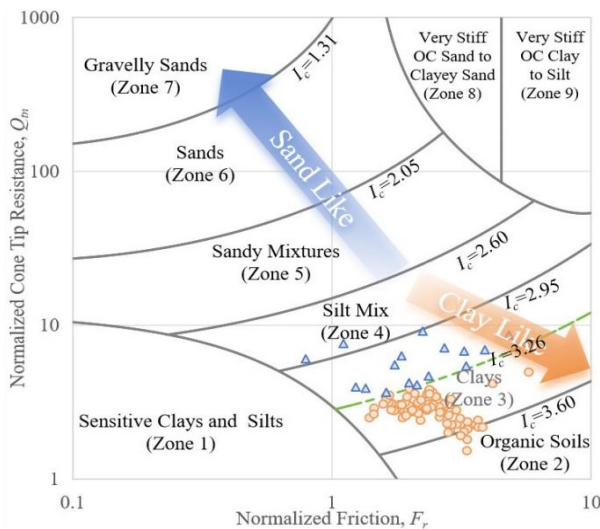


Fig. 6. Classifying the database in the Roberston  $Q_{tn}$  vs.  $F_r$  Chart

Using the aforementioned grouping method, the CPTu data and  $s_u$  values are re-plotted on the coordinate system based on three different correlations and varying lengths of CPTu profile filtering windows, resulting in the outcomes presented in Figure 7. In Figure 7, the subplots within the same row share the same prefix: "A" denotes a CPTu profile filtering window length of  $3L$ , "B" denotes a length of  $2L$ , and "C" denotes a length of  $L$ . Subplots within the same column share the same suffix: the first column uses the correlation relationship from Equation (2), with the x-axis representing  $(q_c - \sigma_{vo})$ ; the second column uses the correlation from Equation (4), with the x-axis representing  $(q_t - \sigma_{vo})$ ; and the third column uses the correlation from Equation (5), with the x-axis representing  $(q_t - u_2)$ .

After grouping by  $I_c$  values, a distinct separation between the two sets of data points is apparent. Points with  $I_c$  values less than 3.25~3.26 predominantly occupy the region below the boundary line (green dashed line), whereas points with  $I_c$  values greater than 3.25~3.26 are primarily found in the region above the boundary line. Although 2 to 3

points from each group cross the boundary, resulting in a minor overlap in the actual range of cone factors, this overlap can be disregarded. This is because the number of overlapping points is sufficiently minimal compared to the overall dataset. Moreover, this result is largely unavoidable due to factors such as the heterogeneous nature of soil, differences in the spatial distribution of the data, and the pairing method employed. The boundary values for the cone factors can be approximately defined as  $N_k = 13$ ,  $N_{kt} = 14.4$ , and  $N_{ke} = 15$ . Finally, the upper and lower bounds of the cone factor, along with its linear regression value, can be utilized to evaluate the undrained shear stress ( $s_u$ ). The linear regression value is employed to estimate the expected value of  $s_u$  for a given  $I_c$  range, while the bounds could provide a range for  $s_u$ . For instance, in Figure 7-A1, for soil with  $I_c > 3.25$ , the linear regression value of  $N_k$ ,  $\bar{N}_k$  is 8.54, with a range of 5.13 to 13; for soil with  $I_c < 3.25$ , the linear regression value of  $N_k$ ,  $\bar{N}_k$  is 22.42, with a range of 13 to 59.86. The error margin is narrower when the data is assessed by classification among soil classes, in contrast to Figure 5, where no such distinction is made. The group of blue points with  $I_c < 3.25 \sim 3.26$  shows a broader range of cone factors and a more scattered distribution, lacking a clear linear relationship. This may be attributed to two factors: first, there are fewer data points within this  $I_c$  range; second, the soil in this group displays more silt-like characteristics. In contrast, the group of orange points with  $I_c$  values greater than 3.25~3.26 exhibits more pronounced clay-like characteristics, resulting in a much narrower range of cone factors and a distribution that aligns more closely with a linear relationship. As a result, the  $s_u$  values for this group can be predicted with greater accuracy.

Based on Figure 7, a comparison of the three correlations—Equations (2), (4), and (5)—reveals that using  $(q_t - u_2)$  yields a significantly weaker linear correlation for predicting  $s_u$  compared to the other two methods. This diminished performance could be attributed to the overwhelming influence of pore-water pressure ( $u_2$ ). Additionally, Equation (4) slightly outperforms Equation (2), likely due to its more effective consideration of pore-water pressure through the corrected cone tip resistance ( $q_t$ ).

When evaluating the impact of different filtering window lengths, it is observed that for points with  $I_c > 3.25 \sim 3.26$ , the linear correlation results are minimally affected. Conversely, for points with  $I_c < 3.25 \sim 3.26$ , the smallest filtering window length,  $L$ , provides correlations that are more accurate than those obtained with larger window lengths. This discrepancy can be attributed to the fact that, as shown in Figure 4, soil with  $I_c < 3.25 \sim 3.26$  exhibits more silt-like characteristics, leading to greater variation in their CPTu reading profiles and substantial differences in mean values across different filtering window lengths. Therefore, the smallest length,  $L$ , is likely to offer the most accurate reflection of the soil properties at their respective locations.

## 4 Conclusions

This study investigates the correlation between CPTu (piezocone penetration test) results and undrained shear strength ( $s_u$ ) obtained by in-situ vane shear tests for clays in Macau. Our findings demonstrate that:

1. The cone factors describing the correlations between the CPTu readings and  $s_u$  would exhibit significant variability without soil classification. Correlations after soil classification yield a narrower error margin, indicating that it can improve the accuracy of  $s_u$  predictions.

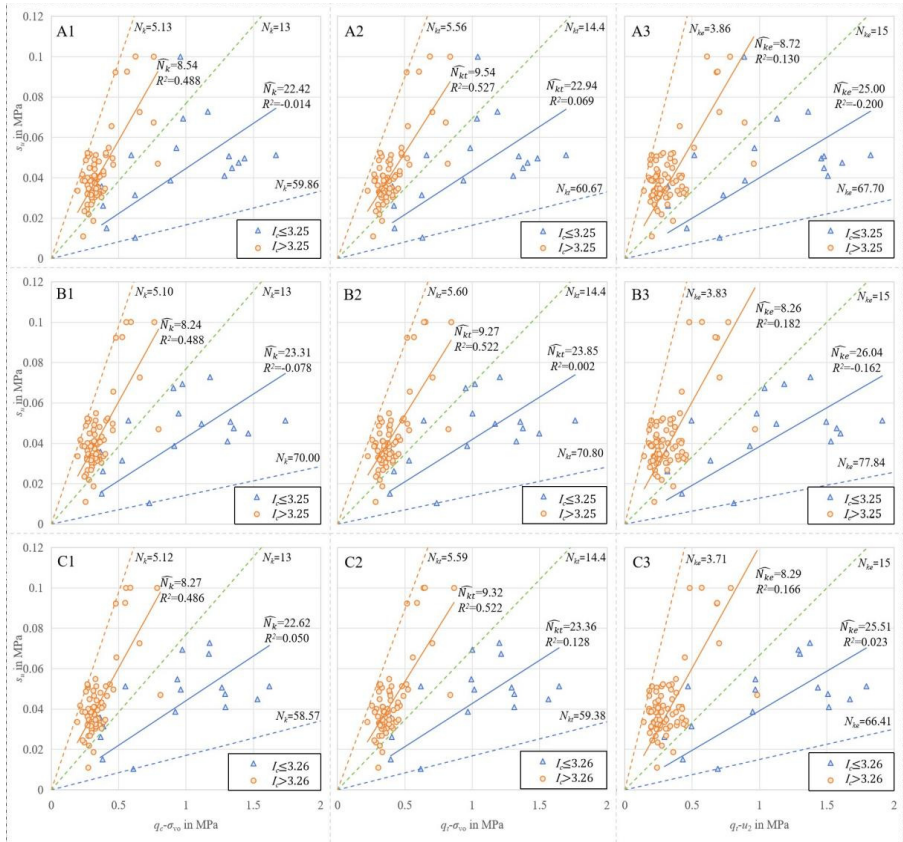


**Fig. 7.** Correlations between the  $s_u$  and different CPTu readings

2. Soil classification can be based on the Soil Behavior Type Index ( $I_c$ ) proposed by Robertson and Wride [25]. For clayey soils in the coastal region of Macau in this paper, it is recommended to categorize the soil into two groups: those with  $I_c > 3.25 \sim 3.26$  and those with  $I_c < 3.25 \sim 3.26$ . The former group has a narrow range of cone factors and high accuracy in predictions of  $s_u$  by using CPTu data. In contrast, the latter group exhibits a broader range of cone factors, which may lead to less accurate predictions.
3. Among the correlation methods studied, using the effective cone tip resistance ( $q_t - u_2$ ) results in a much weaker linear correlation for predicting  $s_u$ , which would be not recommended to interpret undrained shear stress by CPTu. Between the other

two correlations, net cone tip resistance ( $q_t - \sigma_{vo}$ ) has slightly better performance than total cone tip resistance ( $q_c - \sigma_{vo}$ ) in terms of prediction accuracy.

4. For soil with  $I_c > 3.25 \sim 3.26$ , the choice of filtering window length had minimal impact on the correlation results. However, for soil with  $I_c < 3.25 \sim 3.26$ , the smaller filtering window length ( $L$ ) provided more accurate correlations. Therefore, it is recommended that the length of the CPTu reading profile used for interpretation should match the length of the shear vane.

Despite these insights, the study acknowledges limitations: for soil with  $I_c > 3.25$ , significant variability in cone factors still poses challenges for accurately interpreting  $s_u$  from CPTu tests. Expanding the database and refining soil classification may help mitigate this limitation. On the other hand, establishing a robust linear correlation for CPTu interpretation significantly constrains the applicable range of soil types. Linear regression analysis method is merely a stopgap measure, a compromise made due to either the insufficient robustness of our nonlinear analysis tools or the convenience it offers in practical applications. Future geotechnical researchers should aim to overcome this compromise by leveraging advanced tools and models, such as neural network algorithms, to address nonlinear challenges in engineering.

**Supplementary Materials:** The following supporting information can be downloaded at: <https://drive.google.com/drive/folders/1ssMdYV5rMpwmGqyp5-zTnfl6y9z7FUUu?usp=sharing>, Table S1: VST data summary; Table S2: CPTu data summary (equal step length), Table S3: distance weights.

## Acknowledgment

**Funding:** This research was funded by Ministry of Housing and Urban-Rural Development, PRC, Science and Technology Plan Projects, grant number: 2022-K-039; Guangdong Province Department of Housing and Urban-Rural Development, Science and Technology Plan Projects, grant number: 2020-K5-144658; Guangzhou Municipal Construction Group Co., Ltd., Science and Technology Plan Projects, grant number: 2021-KJ006 and 2024-KJ084; Guangzhou Design Institute Group Co., Ltd., Science and Technology Plan Projects, grant number: 24RD22-B1, 24RD23-B1 and 24RD24-B1.

## References

1. Mayne, P. W.; Peuchen, J. Evaluation of CPTU  $N_{kt}$  Cone Factor for Undrained Strength of Clays. In Cone Penetration Testing 2018, Proceedings of the 4th International Symposium on Cone Penetration Testing (CPT'18), Netherlands, 21-22 June 2018.
2. Wang, Z.-L.; Chen, H.-B.; Chen, F.-Q.; Liu, L.-Y. Determination of the Overconsolidation Ratio and Undrained Shear Strength of Cohesive Soils by CPTu Measurement. *Appl. Ocean Res.* **2024**, *146*, 103949.
3. Lunne, T.; Robertson, P. K.; Powell, J. J. M. In Cone Penetration Testing in Geotechnical Practice, 1<sup>st</sup> ed.; CRC Press: London, UK, 1997; Chapter 5, pp. 63-68, ISBN 978-042-917-780-4.

4. Mayne, P. W., Benoit, J. Analytical CPTu Models Applied to Sensitive Clay at Dover, New Hampshire. *J. Geotech. Geoenviron. Eng.* **2020**, 146(12): 04020130.
5. Mo, P. Q., Gao, X. W., Yang, W., & Yu, H. S. A Cavity Expansion–Based Solution for Interpretation of CPTu Data in Soils under Partially Drained Conditions. *Int. J. Numer. Anal. Methods Geomech.* **2020**, 44(7), 1053-1076.
6. Mo, P. Q., Cai, G. J., Wang, K. J., Eslami, A., & Yu, H. S. Cavity Expansion-Based Interpretation of Piezocone Penetration test (CPTu) Data in Clays. *Géotechnique*, **2024**, 1(20).
7. Baligh, M. M. Strain Path Method. *J. Geotech. Eng.* **1985**, 111 (9), 1108–1136.
8. Khosravi, A., Martinez, A., Dejong, J. T. Discrete Element Model (DEM) Simulations of Cone Penetration Test (CPT) Measurements and Soil Classification. *Can. Geotech. J.* **2020**, 57: 1369-1387.
9. Pezeshki, A. Ahmadi, M. M. In Situ State of Tailing Silts Using a Numerical Model of Piezocone Penetration Test Developed by Norsand Model. *Int. J. Geomech.*, **2022** 22(1), 04021264.
10. Song, Z., Truby, R., & Luo, S. Selection of Soil Shear Strength Parameters Based on Integrated in situ Tests, Lab Tests and Numerical Calibration Approach. In *Mine Waste and Tailings Conference 2023*, Brisbane, Australia, 13-14 July, 2023.
11. Bol, E., Önalp, A., Özocak, A., & Sert, S. Estimation of the Undrained Shear Strength of Adapazari Fine Grained Soils by Cone Penetration Test. *Eng. Geol.* **2019**, 261, 105277.
12. Tian, M., Sheng, X. CPT-Based Probabilistic Characterization of Undrained Shear Strength of Clay. *Adv. Civ. Eng.* **2020**, 1, 9617698.
13. Eslami, A., Moshfeghi, S., Molaabasi, H., & Eslami, M. M. In Piezocone and cone penetration test (CPTu and CPT) applications in foundation engineering. Butterworth-Heinemann, 2019, pp. 81-110. ISBN:978-0-08-102766-0.
14. Golestani Dariani, A. A., & Ahmadi, M. M. CPT Cone Factor: Numerical-Analytical Approach. *Int. J. Geomech.* **2019**, 19(12), 04019132.
15. Briggs, K. M., Trinidad González, Y., Powrie, W., Butler, S., & Sartain, N. Quantifying CPT Cone Factors in Clays Derived from Weathered Mudstone. *Q. J. Eng. Geol. Hydrogeol.* **2024**, 57(1), qjeh2023-014.
16. Kulhawy, F. H.; Mayne, P. W. *Manual on Estimating Soil Properties for Foundation Design*; Electric Power Research Inst.: Palo Alto, CA USA; Cornell Univ.: Ithaca, NY USA, 1990.
17. Jamiolkowski M.; Ladd, C. C.; Germaine, J. T.; Lancellotta, R. *New Developments in Field and Laboratory Testing of Soils*. In 11th International Conference on Soil Mechanics and Foundation Engineering, Vol.1, Proceedings of the 11<sup>th</sup> International Conference on Soil Mechanics and Foundation Engineering, San Francisco, CA, USA, 12-16 Aug. 1985.
18. BS 1377, B. S. *Methods of Test for Soils for Civil Engineering Purposes*. British Standards Institution, London, UK 1990.
19. ASTM D5778–20, *Standard Test Method for Electronic Friction Cone and Piezocone Penetration Testing of Soils*. ASTM Committee, West Conshohocken, PA, US 2020.
20. Campanella, R. G.; Gillespie, D.; PK, R. *Pore Pressures during Cone Penetration Testing*. In Proceedings of the ESOPT II 2<sup>nd</sup> European Symposium on Penetration Testing, Amsterdam, Netherlands, 24-27, May, 1982.
21. Senneset, K.; Sandven, R.; Janbu, N. Evaluation of Soil Parameters from Piezocone Tests. *Transp. Res. Rec.* **1989**, No. 1235, 24-37.
22. Sowers, G. F. *Introductory Soil Mechanics & Foundations*, 4<sup>th</sup> ed. Macmillan: New York, NY, USA, 1979; p. 621.
23. Jefferies, M. G.; Davies, M. P. Use of CPTu to Estimate Equivalent SPT<sub>N60</sub>. *Geotech. Test. J.* **1993**, 16 (4), 458–468.

24. Been, K.; Jefferies, M. G. Towards Systematic CPT Interpretation. In Predictive Soil Mechanics, Proceedings of the Wroth Memorial Symposium, St Catherine's College, Oxford, UK, 27-29 July 1992; Telford, T. Publishing, London, UK, 1992; pp. 121-134.
25. Robertson, P. K.; Wride, C. E. Evaluating Cyclic Liquefaction Potential Using the Cone Penetration Test. *Can. Geotech. J.* **1998**, *35* (3), 442–459.
26. Robertson, P. K. Interpretation of Cone Penetration Tests—A Unified Approach. *Can. Geotech. J.* **2009**, *46* (11), 1337–1355.
27. Zhang, G.; Robertson, P. K.; Brachman, R. W. Estimating Liquefaction-Induced Ground Settlements from CPT for Level Ground. *Can. Geotech. J.* **2002**, *39* (5), 1168–1180.
28. Mayne, P. W.; Woeller, D. J. Generalized Direct CPT Method for Evaluating Footing Deformation Response and Capacity on Sands, Silts, and Clays. In Geo-characterization and Modeling for Sustainability, Proceedings of Geo-congress 2014, Atlanta, Georgia, USA, 23-26, Feb., 2014.
29. Tobler, W. R. A Computer Movie Simulating Urban Growth in the Detroit Region. *Econ. Geogr.* **1970**, *46* (sup1), 234–240.
30. Macedo, J., Mayne, P. W., Dai, S., Torres, P., Arnold, C., Vergaray, L., & Zhao, Y. Cone Penetration Testing for Illinois Subsurface Characterization and Geotechnical Design (No. FHWA-ICT-24-011). Illinois Center for Transportation, **2024**.

**Open Access** This chapter is licensed under the terms of the Creative Commons Attribution-NonCommercial 4.0 International License (<http://creativecommons.org/licenses/by-nc/4.0/>), which permits any noncommercial use, sharing, adaptation, distribution and reproduction in any medium or format, as long as you give appropriate credit to the original author(s) and the source, provide a link to the Creative Commons license and indicate if changes were made.

The images or other third party material in this chapter are included in the chapter's Creative Commons license, unless indicated otherwise in a credit line to the material. If material is not included in the chapter's Creative Commons license and your intended use is not permitted by statutory regulation or exceeds the permitted use, you will need to obtain permission directly from the copyright holder.

